Since January 2020 Elsevier has created a COVID-19 resource centre with free information in English and Mandarin on the novel coronavirus COVID-19. The COVID-19 resource centre is hosted on Elsevier Connect, the company's public news and information website.

International Journal of Biological Macromolecules 200 (2022) 438–448

Contents lists available at ScienceDirect

International Journal of Biological Macromolecules

journal homepage: www.elsevier.com/locate/ijbiomac

The Omicron (B.1.1.529) variant of SARS-CoV-2 binds to the hACE2 receptor more strongly and escapes the antibody response: Insights from structural and simulation data

Abbas Khan [a], Hira Waris [b], Memoona Rafique [c], Muhammad Suleman [d], Anwar Mohammad [e], Syed Shujait Ali [d], Taimoor Khan [a], Yasir Waheed [f], Chenguang Liao [g], Dong-Qing Wei [a,h,i,*]

[a] Department of Bioinformatics and Biological Statistics, School of Life Sciences and Biotechnology, Shanghai Jiao Tong University, Shanghai 200240, PR China
[b] Rawalpindi Medical College, Rawalpindi, Punjab, Pakistan
[c] King Edward Medical University, Lahore, Punjab, Pakistan
[d] Center for Biotechnology and Microbiology, University of Swat, Khyber Pakhtunkhwa, Pakistan
[e] Department of Biochemistry and Molecular Biology, Dasman Diabetes Institute, Kuwait
[f] Foundation University Medical College, Foundation University Islamabad, Islamabad, Pakistan
[g] College of Software, Zhengzhou University, Daxue Road, Zhengzhou, China
[h] State Key Laboratory of Microbial Metabolism, Shanghai-Islamabad-Belgrade Joint Innovation Center on Antibacterial Resistances, Joint Laboratory of International Laboratory of Metabolic and Developmental Sciences, Ministry of Education and School of Life Sciences and Biotechnology, Shanghai Jiao Tong University, Shanghai 200030, PR China
[i] Peng Cheng Laboratory, Vanke Cloud City Phase I Building 8, Xili Street, Nashan District, Shenzhen, Guangdong 518055, PR China

ARTICLE INFO

Keywords:
Omicron
Docking
Simulation
Dissociation constant
Binding free energy

ABSTRACT

As SARS-CoV-2 (severe acute respiratory syndrome coronavirus 2) continues to inflict chaos globally, a new variant officially known as B.1.1.529 was reported in South Africa and was found to harbor 30 mutations in the spike protein. It is too early to speculate on transmission and hospitalizations. Hence, more analyses are required, particularly to connect the genomic patterns to the phenotypic attributes to reveal the binding differences and antibody response for this variant, which can then be used for therapeutic interventions. Given the urgency of the required analysis and data on the B.1.1.529 variant, we have performed a detailed investigation to provide an understanding of the impact of these novel mutations on the structure, function, and binding of RBD to hACE2 and mAb to the NTD of the spike protein. The differences in the binding pattern between the wild type and B.1.1.529 variant complexes revealed that the key substitutions Asn417, Ser446, Arg493, and Arg498 in the B.1.1.529 RBD caused additional interactions with hACE2 and the loss of key residues in the B.1.1.529 NTD resulted in decreased interactions with three CDR regions (1–3) in the mAb. Further investigation revealed that B.1.1.529 displayed a stable dynamic that follows a global stability trend. In addition, the dissociation constant (K_D), hydrogen bonding analysis, and binding free energy calculations further validated the findings. Hydrogen bonding analysis demonstrated that significant hydrogen bonding reprogramming took place, which revealed key differences in the binding. The total binding free energy using MM/GBSA and MM/PBSA further validated the docking results and demonstrated significant variations in the binding. This study is the first to provide a basis for the higher infectivity of the new SARS-CoV-2 variants and provides a strong impetus for the development of novel drugs against them.

1. Introduction

SARS-CoV-2, which causes the COVID-19 disease, emerged in 2019, and transmission was reported to occur through the contact of healthy individuals with the diseased person [1]. Research has also shown that the virus can rapidly transmit through aerosol and solid surfaces [3,4,5]. Although SARS-CoV-2 exhibits proofreading capabilities when performing viral replication, the exponential spread of this virus has led to a

* Corresponding author at: Department of Bioinformatics and Biological Statistics, School of Life Sciences and Biotechnology, Shanghai Jiao Tong University, Shanghai 200240, PR China.
E-mail address: dqwei@sjtu.edu.cn (D.-Q. Wei).

https://doi.org/10.1016/j.ijbiomac.2022.01.059
Received 5 December 2021; Received in revised form 10 January 2022; Accepted 10 January 2022
Available online 19 January 2022

high frequency of mutations [2,3]. Consequently, the newly reported viral variants can enter into host cells more efficiently and evade the host's immune reaction [4,5].

Since the WHO declared COVID-19 a global pandemic in March 2020, it has ravaged the social fabric and economy worldwide. COVID-19 has overwhelmed healthcare systems around the world. The pandemic's protracted shutdowns have led to a loss of jobs, which has had a ripple effect on the global economy. While considerable advances in clinical research have led to a better understanding of SARS-CoV-2 and the treatments for COVID-19, thus restricting the virus, the emergence of new variants, such as B.1.1.7, B.1.351, P.1, B.1.617, and B.1.618, have been reported around the world and are a growing concern. As SARS-CoV-2 continues to inflict chaos globally, many countries are experiencing a fourth or fifth wave of the pandemic, accredited principally due to the appearance of novel variants of the virus. Recently, many variants have been reported, among which the VOC Delta (δ) + (AY.1 or lineage B.1.617.2.1), which evolved from the Delta variant, has demonstrated a different mutational landscape by acquiring L452R and T478K mutations in the receptor-binding domain (RBD). Meanwhile, the δ + variant acquired an additional mutation, K417N, along with the L452R and T478K mutations [6]. In January 2021, the δ variant was discovered in Colombia and was reported to increase COVID-19 cases. This variant harbors E484K, N501Y, and P681H mutations in the spike protein, which have been accompanied by many other new mutations, including R346K, Y144T, Y145S, and 146N insertion [7]. Moreover, a novel variant of interest (VOI) known as C.37, or the Lambda (λ) variant was found in Peru with mutations L452Q and F490S in the RBD and is suspected to be associated with decreased antibody neutralization susceptibility, particularly due to the F490S mutation in the RBD [8,9]. The Kappa (κ) variant, also known as B.1.617.1, was first identified in India. This VOI has a single mutation, L452R, which is thought to be involved in reduced antibody neutralization by disrupting the respective conformational epitopes [10]. Another VOI known as Iota (ι) from the lineage B.1.526 was observed in New York City in early 2021 and has the E484K mutation found in the P.1 variant. Research has shown that this variant partially or wholly escapes the response of the two currently used therapeutic monoclonal antibodies (mAb) and is less susceptible to neutralization [11]. The E484K substitution in the P.1 variant has been reported to establish a direct interaction with the host receptor hACE2 [12]. A novel variant C.12 has recently been reported in South Africa, but as no associated risks have yet been confirmed, it is currently designated a variant under monitoring [13].

As a result, the introduction of variants has presented a grave threat to the effectiveness of the vaccines that have already been developed. The current SARS-CoV-2 strain (B.1.1.529) that emerged in South Africa in early November and is spreading to other counties has created a distressing public health concern. The B.1.1.529 SARS-CoV-2 variant strain exhibits a total of 30 substitutions in the spike protein. Among these 30 mutations, seven substitutions (A67V, T95I, G142D, N211I, L212V, V213P, and R214E) and two deletions (Δ69–70 and Δ143–145) have been observed in the NTD, while 15 substitutions (G339D, S371L, S373P, S375F, K471N, N440K, G446S, S477N, T478K, E484A, Q493R, G496S, Q498R, N501I, and Y505H) have been found in the RBD. The B.1.1.529 spike protein has been found in previous strains, including novel variants, might alter the transmission and infection of SARS-CoV-2. A report published using epidemiology modeling by employing the S-gene target failure Data (SDFT) revealed that the rate and frequency of the B.1.1.529 variant will be 100-fold higher than the Delta variant previously reported to be the most disastrous variant of SARS-CoV-2 [14]. In Canada this approach has been used for the detection of Omicron variant in a highly infected population, which shows that S-gene based diagnostic can be used for the detection and confirmation of Omicron variant prior to whole genome sequencing [15]. Consequently, the efficacy of the developed vaccines may be reduced and would thus not work against B.1.1.529. For instance Hesperidin, Chrysin,Emodin, Anthraquinone, rhein and many other therapeutics are reported to block the RBD domain and other proteins of SARS-CoV-2 using computational modeling tools [16–18]. To date, 26 approved vaccines are being administered to control the spread of the SARS-CoV-2 virus, in addition to two FDA-approved drugs from Pfizer and Merk. The vaccines have predominately been developed to target the spike protein, on which the B.1.1.529 strain possesses an unprecedented number of mutations, particularly on the RBD domain that binds to ACE2 and the NTD domain where the monoclonal antibodies interact. As such, the international community is scrambling to determine if these mutations in the B.1.1.529 strain will help the virus evade the vaccines. A detailed investigation of these mutations is therefore essential for understanding the impact of the reported substitutions in the B.1.1.529 variant and deciphering the structural changes caused by these mutations, the functional consequences, and the binding variations (RBD-ACE2 and NTD-mAb).

The current study employed protein-protein docking and all-atoms simulation protocols to decipher the mechanism of pathogenesis of the B.1.1.529 variant by comparing it with the wild type. This study revealed two different aspects of pathogenesis: first, we investigated the interaction of the RBD with hACE2 to determine the binding differences between the variant and the wild type (Wuhan strain), and second, we examined the binding of monoclonal antibodies (4A8) to the NTD of the spike protein to understand immune evasion. Furthermore, we explored the structural dynamic features and hydrogen bonding networks on the spike protein of the wild type and B.1.1.528 variant RBD and NTD domains in complex with ACE2 and mAb, respectively, to understand key dynamic variations. In addition, we calculated the binding affinity of each complex using molecular mechanics/generalized born surface area (MM/GBSA). Our analysis revealed that the B.1.1.529 variant enables a more robust binding of the RBD with hACE2 than the wild type and reduces the binding at NTD.

2. Methodology

2.1. Retrieval of data and mutant modeling

Recently the omicron (B.1.1.529) SARS-CoV-2 variant of concern was reported in South Africa and claimed to be very contagious. Infections have risen sharply in recent weeks, correlating with the discovery of the B.1.1.529 strain. A specimen taken on November 9, 2021, was the first reported verified case of COVID-19 infection caused by B.1.1.529 variant of the SARS-CoV-2 [19]. More than thirty mutations were detected in the spike protein of this novel strain. As spike protein is very important in the first step of viral pathogenesis, we retrieved the recently uploaded SARS-CoV-2 spike protein amino acid sequence using accession ID: P0DTC2 from UniProt to model the reported mutations on the correct location [20]. Afterward, the reference structure of SARS-CoV-2 spike protein (6M0J) reported in Wuhan, China, was retrieved from the PDB online database, which was used as template for structural modeling of the mutant [21,22]. The NTD of the spike protein in complex with monoclonal antibodies (4A8) was retrieved from RCSB using 7C2L accession number [23]. Finally, the Chimera software was used to model the recently reported mutations in the wild-type structure of spike protein RBD and NTD [24,25].

2.2. Restraint docking of wild-type and mutant spike protein and ACE2

The HADDOCK (high ambiguity-driven protein-protein docking) algorithm [26,27] was used to perform the restraint docking of wild-type and B.1.1.529 with ACE2 receptor by defining the interface residues as reported previously [12,28,29]. For RBD and NTD, restraint docking was performed by determining the interface residues as 21, 24, 27, 28, 30, 35, 38, 79, 80, 82, 83, and 353 for ACE2, and at 449, 453, 455, 456, 486, 487, 489, 493, 496, 498, 500, 501, 502, and 505 for RBD while for NTD the interface residues as 25–32, 51–58, and 100–116 for mAbs, and at 145–150 for NTD were defined as binding site. The protonation state

is set by default by the new HADDOCK 2.4 version which was left as *(autohis = true)*. The membrane *Z*-positioning restraints was set default which is an experimental type of restraints in HADDOCK2.4. For Ambiguous (AIRs) and unambiguous distance restraints, a semi-flexible simulated annealing (SA) approach was used. The surface contacts restraint was set on *(surfrest = true)* while the dihedral angle restraints was set by default. To visualize the interaction interface between the spike protein and ACE2, we used the Guru interface, which is managed by the HADDOCK server and can perform the protein-protein or protein-RNA/DNA docking. To find out the interaction pattern like electrostatic, hydrogen, and salt bridge, we used the PDBsum online server [30]. Understanding the structural determinants of protein complexes is crucial for gaining a better understanding of biological activities, pathologies, and therapeutic discovery. The potential to precisely estimate the binding affinity of a protein-protein complex is a crucial part of this. For prediction of the binding strength of these complex dissociation constant (KD) is considered as the best approach to forecast the binding. Herein, for this purpose PRODIGY (PROtein binDIng enerGY prediction) https://wenmr.science.uu.nl/prodigy/ was used.

2.3. Molecular dynamics simulation of wild-type and mutant complexes

The AMBER20 package was used to perform molecular dynamics (MD) simulation to check the dynamic behavior of both wild-type and B.1.1.529 RBDs with the ACE2 receptor using FF19SB force field [31–33]. An OPC water box that has been reported to have higher accuracy in the FF19SB was used for the system's solvation and sodium counter ions were added for system neutralization. In each system, bad clashes were removed using an energy minimization methodology. Using 6000 cycles for the first step by employing the steepest descent algorithm, while 3000 cycles were used by employing the conjugate gradient algorithm [34,35]. The equilibration of the system was carried out at 1 atm pressure (with both weak restraint and without restraint) after heating the system up to 300 K. The production of each complex was accelerated through PMEMD.CUDA for a total of 500 and 400 ns, respectively [36]. The trajectories were processed using CPPTRAJ and PTRAJ modules [37]. For structural stability root mean square deviation (RMSD) analysis, which is a numerical estimation, demonstrates the difference between a target structure and a reference structure was performed using the following equation.

$$RMSD = \sqrt{\frac{1}{N}\sum_{i=}^{N}\sigma_i^2} \quad \text{(i)}$$

where δi is the distance between atom i and either a reference structure or the mean position of the N equivalent atoms. This is often calculated for the backbone heavy atoms C, N, O, and Cα or sometimes just the Cα atoms.

RMSF (root mean square fluctuation) on the other hand, instead of indicating positional differences between entire structures over time, RMSF is a calculation of residues flexibility, or how a particular residue fluctuates during a simulation [33], mathematically the RMSF can be calculated by using the following equation.

$$RMSF_i = \left[\frac{1}{T}\sum_{t_j=1}^{T}|r_i(t_j) - r_i^{ref}|^2\right]^{1/2} \quad \text{(ii)}$$

where T is the time over which one wants to average and $\mathbf{r}_i^{\text{ref}}$ is the reference position of particle *i*. This reference position will be the time-averaged position of the same particle *i*.

2.4. Estimation of binding free energy

According to the previous studies, the MM/GBSA and MM/PBSA are the best approaches for the estimation of accurate binding energy of various biological complexes such as protein-protein, protein-ligand and protein-RNA/DNA [38–42]. In the present study, we used the MM/GBSA and MM-PBSA approaches to calculate the binding energy of both wild-type and mutant complexes by considering the whole trajectories. Finally, to estimate the total binding energy such as electrostatic, GB, SA and vdW, we used the MMGBSA.py script [43].

The following equation was used for energy calculation:

"$\Delta G(bind) = \Delta G(complex) - [\Delta G(receptor) + \Delta G(ligand)]$"

The above-mentioned component of the total free energy was calculated using the following equation:

"$G = Gbond + Gele + GvdW + Gpol + Gnpol$"

3. Results and discussion

Since COVID-19 emerged as a global pandemic in March 2020, it has posed a serious threat to societies and economies worldwide, putting pressure on healthcare systems and resulting in increased unemployment [44]. While progress in clinical research has led to an increased understanding of SARS-CoV-2 and its treatments, newly emerged variants remain an important concern and have caused multiple waves of the pandemic in several countries. The recent variant B.1.1.529 has 30 mutations on the spike protein, which is the primary means of initiating the infection caused by SARS-CoV-2. The full-length structure and domain organization of the spike protein is shown in Fig. 1A and B. Among the 30 mutations in the spike protein, seven substitutions (A67V, T95I, G142D, N211I, L212V, V213P, and R214E) and two deletions (Δ69–70 and Δ143–145) are reported in the NTD (Fig. 1C). Moreover, 15 substitutions (G339D, S371L, S373P, S375F, K471N, N440K, G446S, S477N, T478K, E484A, Q493R, G496S, Q498R, N501I, and Y505H) are observed in the RBD (Fig. 1D). In regard to the NTD, the two deletions Δ69–70 and Δ143–145 were previously reported in the B.1.618 variant and found to reduce mAb binding to the NTD, thus acting as an antibody escaping variant [29]. Furthermore, important substitutions in the RBD, such as K417N, G446S, S477N, T478K, and N501Y, have also been previously reported in several variants, including B.1.1.7, B.1.351, P.1, B.1.617, and B.1.618. These substitutions increase the binding affinity for the host receptor ACE2, which consequently increases transmission and hospitalizations and diminishes the efficacy of different vaccines [12,28,45–47]. In November 2021, the WHO officially identified B.1.1.529 as a new variant of concern. B.1.1.529 has created a highly worrisome situation because of the ongoing transmission reported in South Africa. According to the model generated with data from the S-gene target failure (SDFT), the rate of infection from B.1.1.529 is 100 times higher than that of the Delta variant [14]. It is not possible to speculate on the transmission, hospitalization, and the vaccine's efficacy due to the lack of sufficient data. We have thus conducted a detailed investigation on the effects of this novel mutation on the structure, function, and binding of the RBD to hACE2 and the mAb to the NTD of the spike protein. The current study uses integrated protein-protein and biophysical simulation approaches to demonstrate the binding differences and correlate them with the infectivity of the newly emerged B.1.1.529 variant. In this regard, we used a comparative modeling approach to perform computational modeling of the RBD and NTD structures of B.1.1.529. Using a modeler embedded in Chimera software, we subjected the variants sequences to molecular modeling, which revealed the correct structures of both the RBD and NTD of the B.1.1.529 variant. A structural comparison of the wild type RBD and NTD with the modeled structures of the B.1.1.529 variant revealed a difference in the RMSD of 0.835 Å for the RBDs of the wild type and B.1.1.529 variant superimposed structures, while the RMSD difference was 0.524 Å for the NTD. This result shows that the structures had passed through secondary structure rearrangement to induce a different approach to binding and infection. The superimposed structures of the wild type RBD, the B.1.1.529 RBD, the wild type NTD, and the B.1.1.529 NTD are shown in

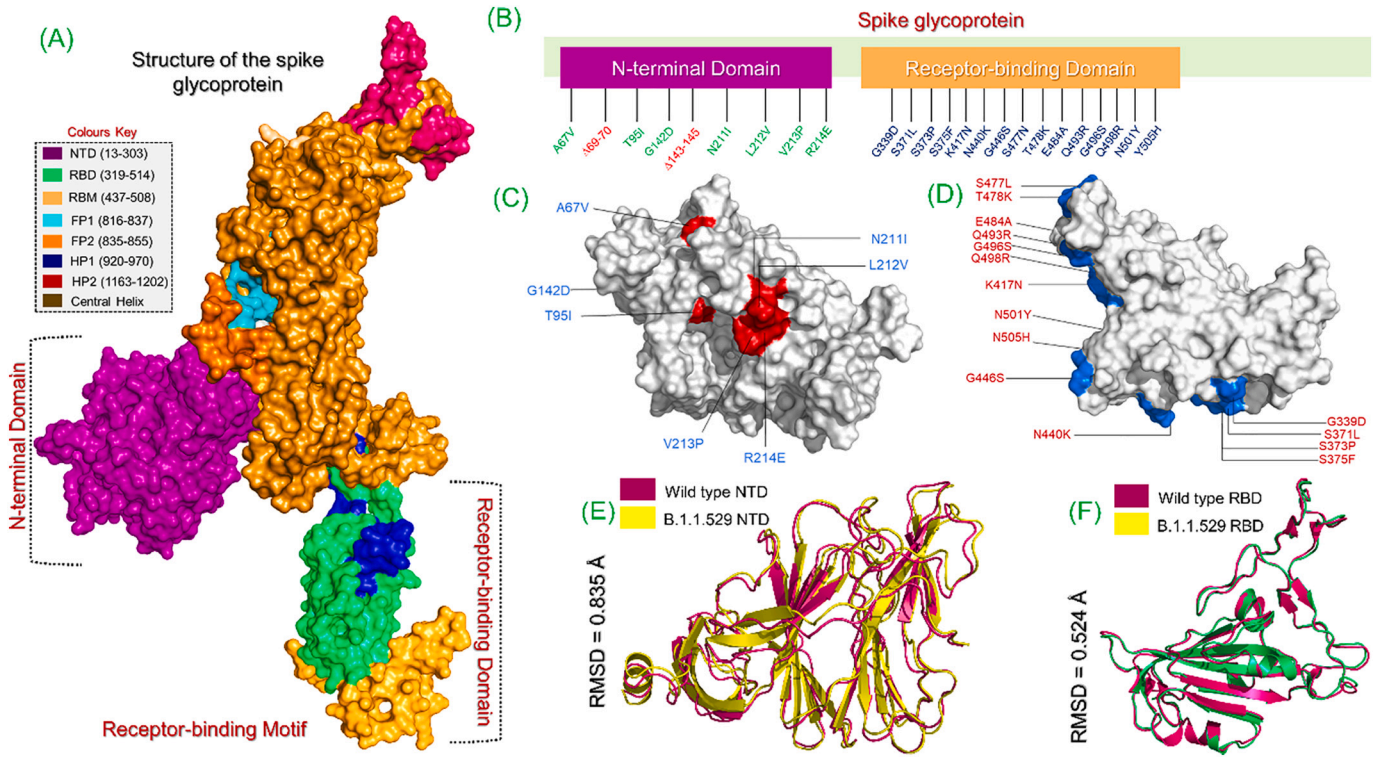

Fig. 1. Structural, domain and mutational organization of the spike glycoprotein of the wild type and B.1.1.529 variant. (A) Shows the domain organization of the spike protein with the two important domains: RBD and NTD are tagged. The RBM in the RBD is coloured orange which comes in direct contact with the hACE2. (B) Show the topographical view and distribution of the mutations and deletions in the RBD and NTD of the spike protein. (C) and (D) represent the reported mutations on the surface of the NTD and RBD. (E) Shows the superimposed structures of the wild type RBD and B.1.1.529 RBD (RMSD = 0.835 Å) while (F) show the superimposed structures of the wild type NTD and B.1.1.529 NTD (RMSD = 0.524 Å).

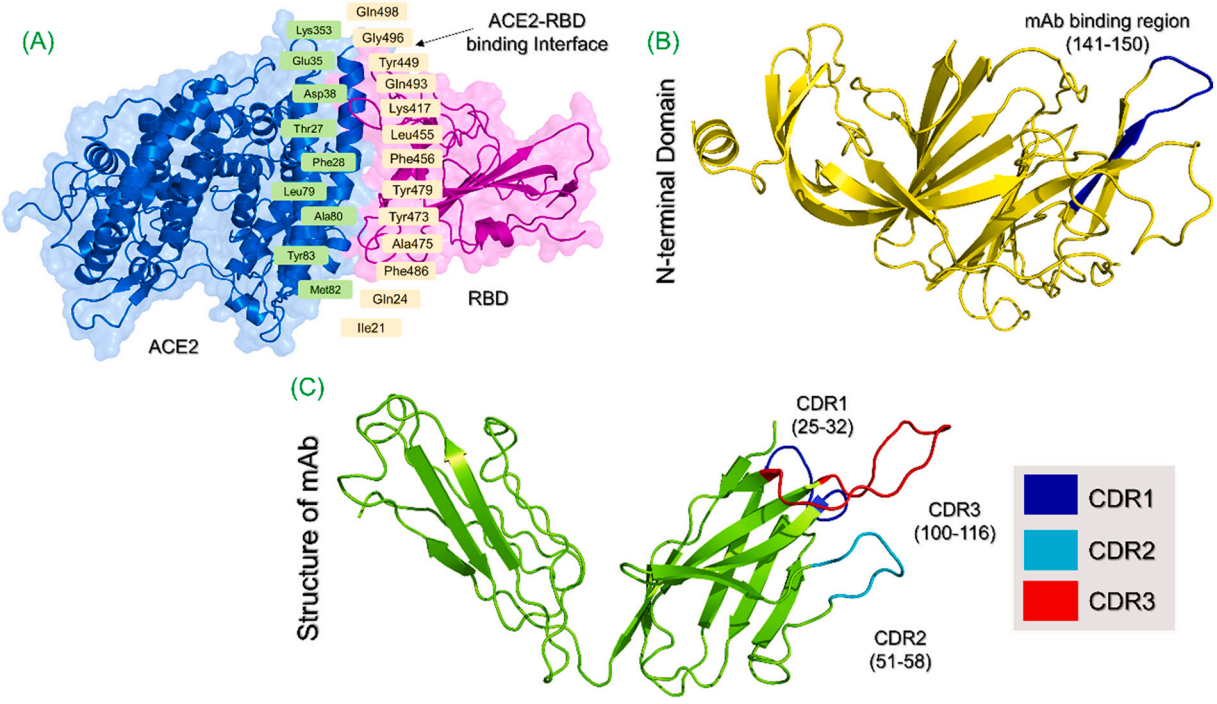

Fig. 2. Structural representation of the interface residues of the hACE2-RBD and NTD-mAb complexes. (A) The interface of the hACE2 and RBD are given where the hACE is coloured as Blue while the RBD is given as Magenta, (B) represent the binding region for mAb on the NTD of the spike protein. The yellow represent the NTD while the blue loop-sheet combination is the binding region. (C) Represent the three CDR regions CDR1 (25–32), CDR2 (51–58) while the CDR3 region (100–116) which interact with the NTD of the spike protein for neutralization. (For interpretation of the references to colour in this figure legend, the reader is referred to the web version of this article.)

Fig. 1E and F.

Next, to predict the protein complexes and reveal the binding differences, a protein-protein docking approach was employed using the HADDOCK web server. Prior to protein-protein docking, the binding interfaces for both domains were identified, and a constraint was applied to achieve accurate docking. The binding interface for RBD and hACE2 is depicted in Fig. 2A. In this regard, a total of nine residues were selected from hACE2, while 13 residues were selected from the RBD for direct interaction with each other. On the other hand, as shown in Fig. 2B, the NTD region 141–150 was selected as the mAb binding site. As Fig. 2C demonstrates, the three important CDR regions, i.e., CDR1 (25–32), CDR2 (51–58), and CDR3 (100–116), were defined as the binding sites for mAb and NTD. The regions are based on previously published studies on both the RBD and NTD [23,45,47].

Using HADDOCK, we predicted the docking score for the wild type-RBD-hACE2 complex as −111.8 ± 1.5 kcal/mol, while the docking score for the B.1.1.529-RBD-hACE2 complex was −118.3 ± 4.9 kcal/mol (Table 1). The data shows that the reported mutations have increased the binding of the B.1.1.529 RBD. The findings follow a similar pattern to that previously reported for other variants (i.e., B.1.1.7, B.1.351, P.1, B.1.617, and B.1.618) where mutations induced a higher docking score for the variants compared to the wild type [12,28,29,47,48]. Moreover, a comparison of the vdW and electrostatic energy values also revealed considerable differences between the wild type and the B.1.1.529 variant. For the wild type, the vdW energy was −48.1 ± 1.3 kcal/mol, while the B.1.1529 variant had a vdW energy of −53.6 ± 8.8 kcal/mol. The electrostatic energy for the wild type and B.1.1.529 variant was −169.7 ± 13.2 kcal/mol and −190.6 ± 36.4 kcal/mol, respectively. Thus, both the vdW energy and the electrostatic energy are increased in the B.1.1.529 variant. Interestingly, a higher electrostatic energy has also been reported in other variants and is considered the primary reason for enhanced binding [12,28,29,47]. To explore the binding differences in detail, we compared the interaction patterns of the wild type and B.1.1.529 variant. The interaction analysis revealed that the wild type exhibited 11 hydrogen bonds and one salt bridge with hACE2, while the B.1.1.529 variant had a total of 12 hydrogen bonds and two salt bridges. This finding shows that, like other variants, the B.1.1.529 variant uses a different approach to interact with hACE2 and increase the transmissibility and infectivity of the virus. As Fig. 3A and B reveal, the interaction between Tyr83 and As487 in both complexes is well conserved, which corroborates with previous findings [12,28,29,47]. *Ismail* et al. also reported this interaction using docking and simulation data [48]. In addition, the important interaction between Glu30 and Lys417, which corresponds to Asn417 in the B.1.1.529 variant, is conserved in both complexes. The only salt bridge in the wild type complex also occurred between Glu30 and Lys417, a finding that is consistent with previous research [48]. In the B.1.1.529 variant, Asn417 is one of the mutated residues and has also been a key mutating hotspot reported in the B.1.351 and P.1 variants [28,45,48]. The interactions between Glu35 and Arg493, one of the mutated residues, were only observed in the B.1.1.529 variant and have previously been shown to be responsible for the anchor locking and correct orientation of the RBD when binding to hACE2 [28,49]. Of the two salt bridges in the B.1.1.529 complex, one is formed by the mutated residue Arg493. This result shows that the mutated residues are directly involved in interactions with hACE2, revealing the functional importance of these substitutions. Moreover, the interaction cluster formed by Lys353 in both complexes reveals the importance of these hotspot residues to enable the RBD to recognize and bind to hACE2 [28,49]. In addition to the other conserved interactions, the two other substitutions, Ser446 and Arg498, were also observed to be in direct contact with hACE2. The second salt bridge was reported between Glu38 and Arg498, which indicates the functional importance of this substitution and the role of Glu38, which has been shown to play a critical role in binding in the wild type and other variants [12,28,29]. The differences in the binding pattern between the wild type and the B.1.1.529 variant complexes revealed that the key substitutions are responsible for enhanced binding and the consequent transmissibility and infectivity. The binding patterns of the wild type and the B.1.1.529-RBD complex are shown in Fig. 3A and B.

We further evaluated the binding differences between the wild type NTD and the B.1.1.529 NTD in complex with the mAb. The HADDOCK docking scores revealed significant variations. For the wild type NTD, the HADDOCK docking score was −63.6 ± 5.2 kcal/mol, while for the B.1.1.529 NTD, the docking score was −51.4 ± 1.9 kcal/mol, which shows substantial differences in the binding induced by the substitutions and deletions in the new variant. Moreover, the interaction analysis revealed that the wild type had seven hydrogen bonds and one salt bridge, while the B.1.1.529 NTD contained only six hydrogen bonds. A further detailed investigation of the interactions demonstrated that the wild type mainly interacts with the three CDR regions (1–3), which are necessary for neutralization. However, in the B.1.1.529 NTD, the interactions were formed only with the CDR1 region, while the other interactions were outside the binding site required for recognition and processing. Furthermore, the three CDR regions in the wild type interact with the correct site on the NTD (region 141–150), while in the B.1.1.529 variant, only the three residues Asn143, Lys145, and Trp147 were involved in the interaction with mAb. No salt bridge was detected in the B.1.1.529-NTD-mAb complex. Research has previously shown that the loss of two important residues, Tyr145 and His146 (particularly His146), decreases the recognition and neutralization of the B.1.618 variant, thus supporting the hypothesis that the deletions of key residues help the virus escape the antibody response and consequently evade neutralization [29]. The interaction patterns of the wild type NTD and the B.1.529 NTD in complex with mAb are shown in Fig. 4A and B.

To further validate the binding differences between the RBD and NTD, we estimated the interaction strength through dissociation constant (K_D) prediction. The strength of a macromolecular complex, particularly the antigen-antibody or protein-protein complex, consistently provides effective data for estimating the binding difference. Previously, this method has been used with different variants to compute the binding strength and reveal the differences between the wild type and different variants (B.1.1.7, B.1.351, P.1, B.1.617 and B.1.618) [12,28,29]. In this study, a similar approach was used to offer insight into the binding strength of the wild type and B.1.1.529 RBDs and NTDs. The results demonstrated that the B.1.1.529 RBD binds more strongly to hACE2 with a K_D value of $1.8E^{-10}$ than the wild type RDB, which has a K_D value of was $3.2E^{-09}$. The current findings strongly corroborate with previous studies that observed stronger binding for different variants than for the wild type [12,28,29]. The K_D was also computed for each complex to determine the impact of the reported

Table 1
Predicted docking scores by HADDOCK, the other parameters including K_D (dissociation constant) for wild type-RBD, wild type-NTD, B.1.1.529-RBD and B.1.1.529-NTD. The bold represent the HADDOCK docking scores.

HADDOCK parameters	Wild type-RBD	B.1.1.529-RBD	Wild Type-NTD	B.1.1.529-NTD
HADDOCK score	**−111.8 ± 1.5**	**−118.3 ± 4.9**	**−63.6 ± 5.2**	**−51.4 ± 1.9**
Cluster size	51	40	9	25
RMSD (Å)	14.6 ± 0.2	0.6 ± 0.4	13.0 ± 0.3	20.5 ± 0.2
Van der Waals energy	−48.1 ± 1.3	−53.6 ± 8.8	−55.2 ± 4.6	−49.4 ± 0.7
Electrostatic energy	−169.7 ± 13.2	−190.6 ± 36.4	−131.8 ± 17.0	−72.7 ± 17.0
De-solvation energy	−30.0 ± 3.4	−27.8 ± 1.7	−1.6 ± 1.7	−14.2 ± 2.8
Restraint's violation energy	1.9 ± 1.1	11.7 ± 13.5	195.5 ± 40.9	267.4 ± 28.1
Buried surface area (A^2)	1661.1 ± 57.7	1690.6 ± 86.1	1341.8 ± 21.7	1305.2 ± 38.9
Z-score	−1.6	−2.4	−1.5	−1.4
K_D (dissociation constant)	$3.2E^{-09}$	$1.8E^{-10}$	$1.9E^{-09}$	$5.8E^{-08}$

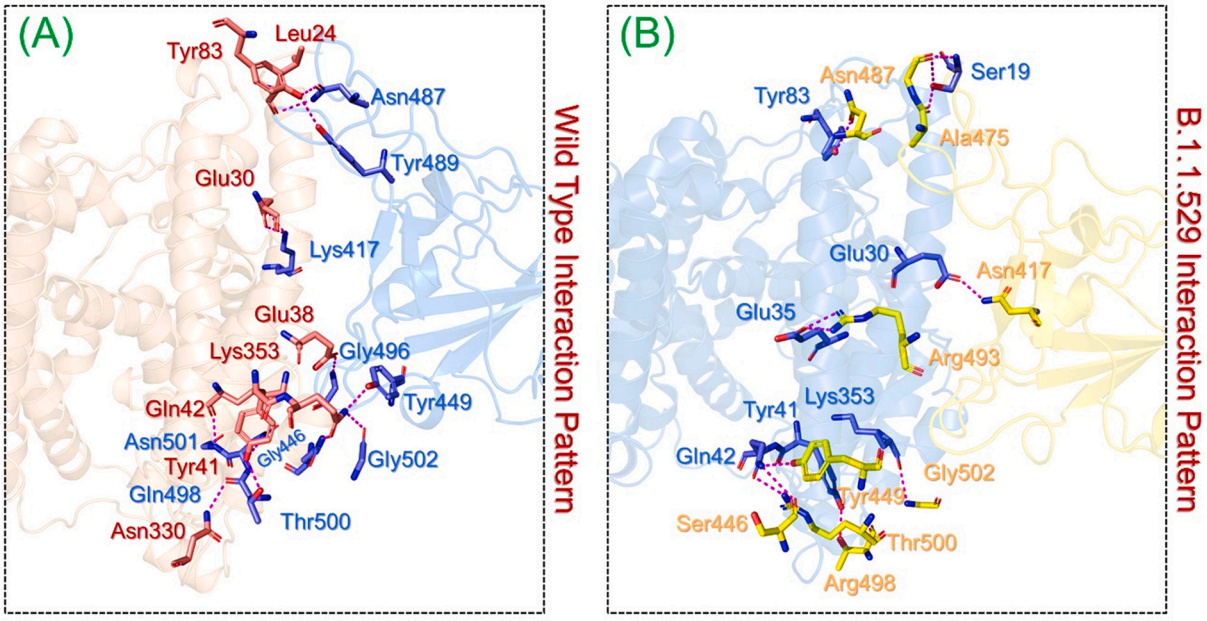

Fig. 3. Comparative interaction analysis of the wild type and B.1.1.529 variant-RBD to the hACE2. (A) represent the interaction of the wild type-RBD with hACE2 while (B) represent the interaction of the B.1.1.529-RBD with hACE2.

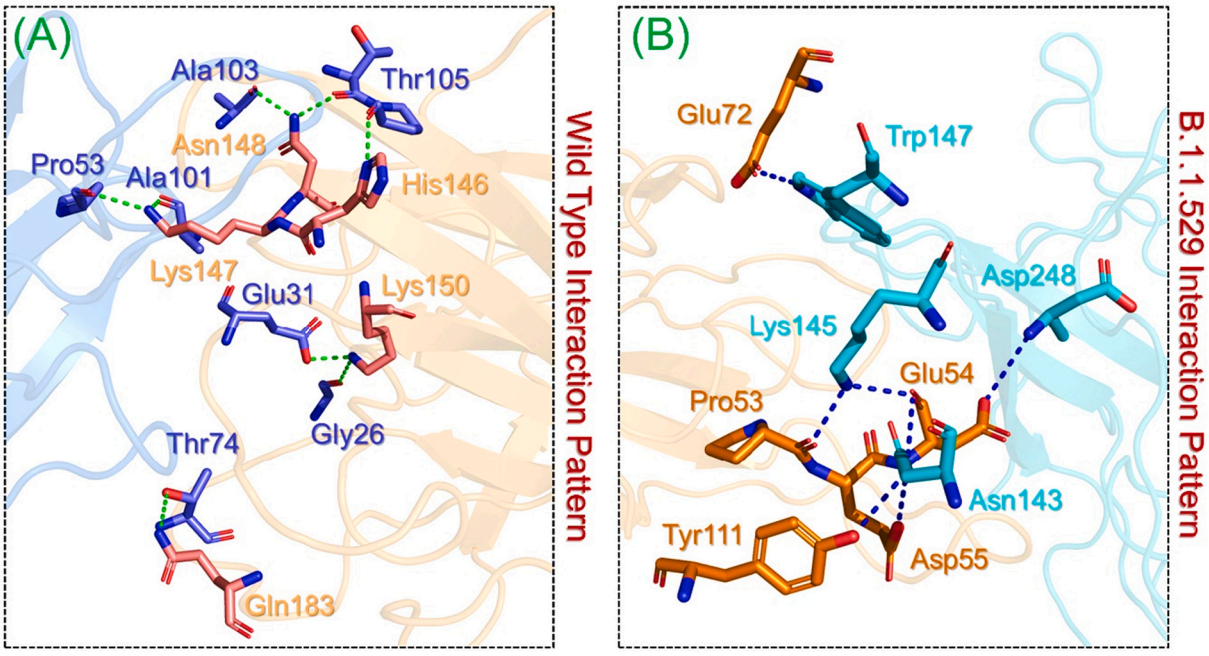

Fig. 4. Comparative interaction analysis of the wild type and B.1.1.529 variant-NTD to the mAb. (A) represent the interaction of the wild type-NTD with mAb while (B) represent the interaction of the B.1.1.529-NTD with mAb.

substitutions and deletions on mAb binding to the NTD. The results revealed that the wild type NTD binds the mAb more strongly than the B.1.1.529 NTD. The K_D was $1.9E^{-09}$ for the wild type and $5.8E^{-08}$ for the B.1.1.529 variant, which shows that the deletions and substitutions at the NTD reduced mAb binding to consequently escape the host's immune response. The docking scores and K_D values for the wild type RBD, wild type NTD, the B.1.1.529 RBD, and the B.1.1.529 NTD are given in Table 1.

An investigation of the structural dynamic features also provides conclusive knowledge regarding the biological function or mechanism of an important cellular process. The use of computational machinery and algorithms to examine the behavior of different biomolecules offers a promising alternative to time-consuming and costly experimental processes. During the pandemic in particular, using such computational methods offers a quick way of devising therapeutic strategies by deciphering the molecular mechanisms of pathogenesis. Thus, to understand the dynamic behaviors and explore the key features of the wild type and the B.1.1.529 variant, we used a molecular dynamics simulation approach. First, we estimated the RMSD for each complex to grasp the impact of the reported substitutions on structural stability and binding. As Fig. 5A shows, both the wild type-RBD-hACE2 and B.1.1.529-RBD-hACE2 complexes exhibited a stable dynamic. Both systems reached

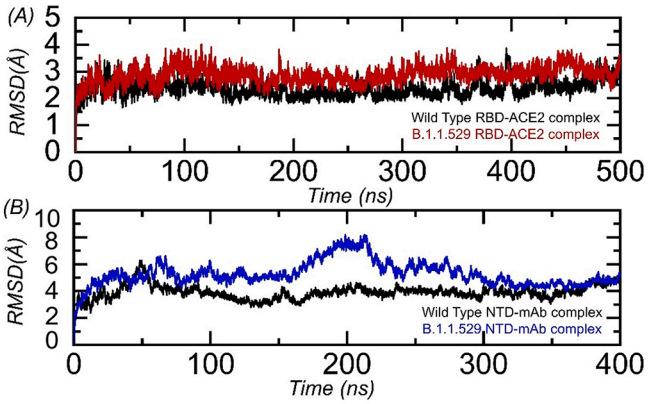

Fig. 5. Structural and dynamic stability of the wild type and B.1.1.529 variant (RBD and NTD). (A) represent the RMSD graph of the wild type and B.1.1.529-RBD in complex with hACE2 while (B) represent the RMSD graph of the wild type and B.1.1.529-NTD with mAb.

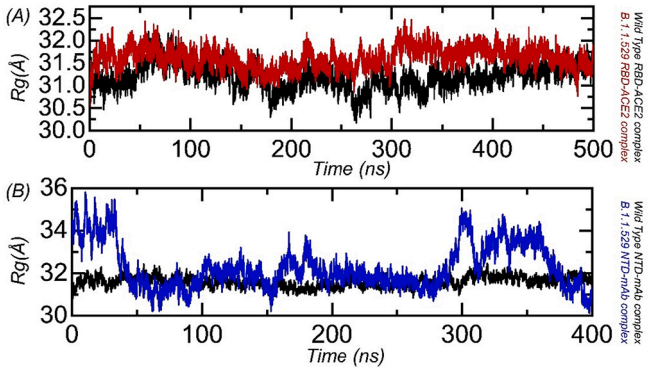

Fig. 6. Structural compactness of the wild type and B.1.1.529 variant (RBD and NTD). (A) represent the Rg graph of the wild type and B.1.1.529-RBD in complex with hACE2 while (B) represent the Rg graph of the wild type and B.1.1.529-NTD with mAb.

the equilibrium points at 50 ns and attained stability at 2.5 Å. Additionally, none of the complexes experienced serious structural perturbation except for the wild type, in which higher deviations between 330 and 400 ns were reported. However, the B.1.1.529-RBD-hACE2 complex exhibited an overall stable dynamic, thus indicating that substitutions in the RBD increase the variant's structural stability and consequently its infectivity. Our findings strongly agree with published research showing that the global stability of the RBD contributes to a higher ACE2 binding affinity [50]. Moreover, previous studies have found a strong correlation between the stability and binding of the RBD, where mutations that increase the structural stability and rigidity accompany increases in binding affinity [51,52]. This finding is further supported by other studies demonstrating that the mutation C432D in the RBD decreased ACE2 assisted entry and destabilized the structure of the RBD [50]. Recently, studies on the variants B.1.1.7, B.1.351, P.1, B.1.617, and B.1.618 also revealed an increase in structural stability that strongly correlates with the stable evolution of variants and tighter binding of other new variants [12,28,29,48]. These results strongly corroborate our findings, which revealed that in addition to a higher binding affinity, the variant's structural stability is also increased, and it thus follows the global trends of stability and higher binding affinity found in other variants. On the other hand, the RMSD values of the wild type-NTD-mAb and B.1.1.529-NTD-mAb complexes demonstrated significantly different RMSD behaviors during the first 250 ns. The RMSD revealed deviations, particularly by the B.1.1.529-NTD-mAb complex, where a higher deviation was experienced between 100 and 250 ns. After this point, both structures demonstrated comparable RMSD values and achieved stability over the simulation time. The NTD and mAb are largely occupied by loops region and the alpha helix and beta sheets which are responsible for the folding stability are available in a minor proportion. Since, the loops are very dynamic in nature so, the deviation of RMSD during the simulation particularly between 1 and 250 ns is due to the widely interspersed loops in the structures. Furthermore, the deletions and mutations also distort the inter-residues network hence producing destabilizing effects. The RMSD values of the wild type-NTD-mAb and B.1.1.529-NTD-mAb complexes are shown in Fig. 5B.

We examined the structural compactness in a dynamic environment by calculating the radius of gyration (Rg) as a function of time. As Fig. 6 indicates, the results of the Rg analysis are consistent with the RMSD results and show a similar structural stability. No significant deviation in the Rg was observed between the wild type-RBD-hACE2 and B.1.1.529-RBD-hACE2 complexes. The complexes displayed very limited binding and unbinding events. The mean Rg for each complex was 31.0 Å and 31.2 Å, respectively. In addition, the Rg values for the wild type NTD and the B.1.1.529 NTD demonstrated significant variations. The wild type presented a uniform Rg with a mean of 31.8 Å. In contrast, the B.1.1.529-NTD-mAb complex initially had a higher Rg value of 35.0 Å between 0 and 50 ns before decreasing between 51 and 150 ns. The Rg then increased again for a short period between 151 and 200 ns, then decreased again and remained consistent until 280 ns. After 281 ns–400 ns, the Rg value experienced significant perturbation. This finding indicates that significant binding and binding events occurred during the simulation of the B.1.1.529-NTD-mAb complex. The Rg values of the wild type-RBD-hACE2 and B.1.1.529-RBD-hACE2 complexes are shown in Fig. 6A, while the Rg graph of the wild type-NTD-mAb and B.1.1.529-NTD-mAb complexes is shown in Fig. 6B.

We gained insight into the residue level fluctuations of the wild type and the variants by examining local level flexibility, which strengthens intermolecular binding, negatively impacts molecular recognition, and can potentially influence the overall function of the biological molecule. A higher and lower RMSF value indicates flexible and stable regions, respectively. Usually, loop regions are more unstable since they do not have a fixed secondary structure and therefore correspond to a higher RMSF. The wild type-RBD-hACE2 and B.1.1.529-RBD-hACE2 complexes demonstrated a similar fluctuation index, whereas the wild type-NTD-mAb and B.1.1.529-NTD-mAb displayed significant variations in residual flexibility. The wild type-NTD-mAb complex exhibited a higher fluctuation for region 250–50aa, while the B.1.1.529-NTD-mAb complex displayed a higher fluctuation between 1–250aa. The differential flexibility index demonstrates variations in conformational optimization and binding strength. The RMSF values of the wild type-RBD-hACE2 and B.1.1.529-RBD-hACE2 complexes and the wild type-NTD-mAb and B.1.1.529-NTD-mAb complexes are shown in Fig. 7A and B.

Macromolecular complexes, particularly protein-protein coupling, are primarily driven by numerous factors, among which hydrogen bonding and hydrophobic contacts are essential. The environment of protein interfaces is enriched with water molecules that work with the residues to form hydrogen bonds [53]. The mechanisms underlying protein-protein interaction, as well as the ramifications for hydrogen bonding, are unclear. [54]. Whether hydrogen bonds govern protein-protein docking in particular is a long-standing concern, and the mechanism is poorly understood [55,56]. Thus, it is important to understand the hydrogen bonding landscape in the protein-protein association. For instance, previously, hydrogen bonding was predicted to estimate the strength of the association between two macromolecules, which shed light on the mechanism of pathogenesis induced by different mutations in SARS-CoV-2 variants, including B.1.1.7 B.1.351, P.1, B.1.617, and B.1.618. Here, we have employed a similar approach to understand the differences in hydrogen bonding between the wild type and B.1.1.529 variant (RBD and NTD) complexes. For the wild type-RBD-hACE2 and B.1.1.529-RBD-hACE2 complexes, the average number of hydrogen bonds was 383 and 387, respectively. Meanwhile, in the

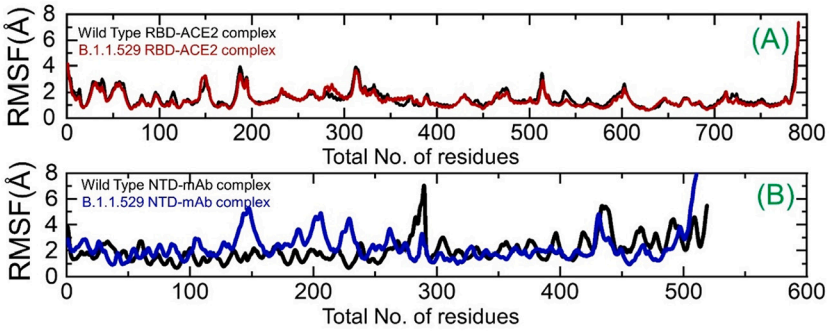

Fig. 7. Residual flexibility index of the wild type and B.1.1.529 variant (RBD and NTD) calculated from the MD trajectories. (A) represent the RMSF graph of the wild type and B.1.1.529-RBD in complex with hACE2 while (B) represent the RMSF graph of the wild type and B.1.1.529-NTD with mAb.

wild type-NTD-mAb complex, the average number of hydrogen bonds was 230, while in B.1.1.529-NTD-mAb, the average number was 215. Similar findings have been previously reported for other variants which also harboured deletions and Mutations in the NTD i.e. B.1.1.618 [28]. This finding shows that the mutations in the RBD help the omicron variant form additional interactions, and significant hydrogen bonding reprogramming took place. Furthermore, in the NTD, the deletions and substitutions led to decreased interactions, particularly with the three CDR regions discussed in the previously mentioned interactions. The hydrogen bonding graphs as a function of time are shown in Fig. 8A and B.

Post-simulation investigation of the average structures from the wild type-RBD and B.1.1.529-RBD simulation trajectories revealed altered hydrogen bonding paradigm. As given in Table 2, the wild type-RBD-ACE2 complex has lost some key interactions while keeping only six hydrogen bonds and only one salt bridge. On the other hand, nine hydrogen bonds and two salt bridges are retained by the B.1.1.529-RBD-ACE2 complex. Interestingly the additional bonds are retained by the mutated residues such as Tyr453, Arg493 and Arg498. The non-bonded contacts in the wild type complex were reported to be 97 while in B.1.1.529-RBD-ACE2 complex 101 non-bonded contacts were observed. This shows the importance of these residues in the evolution of more infective variant (B.1.1.529) of the SARS-CoV-2.

Analysis of the hydrogen bonding and salt-bridges in the NTD of the wild type and B.1.1.529 variant in association with mAb revealed that the wild type-NTD-mAb complex retained five hydrogen bonds and two salt bridges. The extra salt bridges were established during the simulation. The B.1.1.529-NTD-mAb complex reported four hydrogen bonds Arg153-Phe109, Asn143-Tyr111, Lys145-Pro53 and Trp147-Gly56.

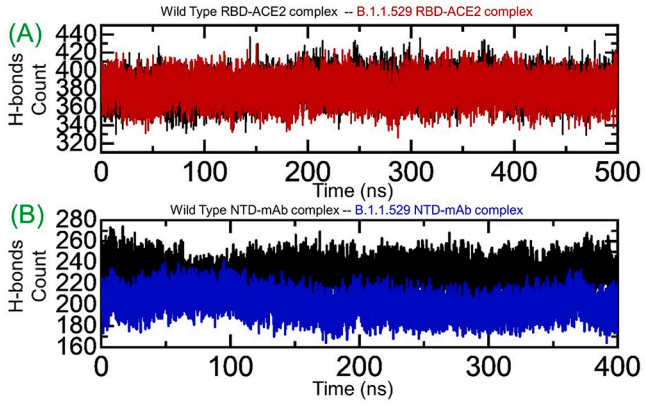

Fig. 8. Hydrogen bonding analysis of the wild type and B.1.1.529 variant (RBD and NTD) complexes. (A) represent the H-bonds count graph of the wild type and B.1.1.529-RBD in complex with hACE2 while (B) represent the H-bonds graph of the wild type and B.1.1.529-NTD with mAb.

Table 2
Post-simulation interactions analysis of the wild type-RBD and B.1.1.529-RBD in complex with ACE2. The table shows the interacting residues, bonding distance and bond type.

Complex name	Interacting residues	Distance (Å)	Bond type
Wild type-RBD	Asn487-Tyr83	2.73	Hydrogen bond
	Ser494-Tyr34	2.67	Hydrogen bond
	Gln498-Tyr41	2.89	Hydrogen bond
	Thr500-Asp355	2.75	Hydrogen bond
	Gly502-Lys353	2.86	Hydrogen bond
	Gly502-Lys353	2.86	Hydrogen bond
	Lys417-Glu30	3.28	Salt-bridge
B.1.1.529-RBD	Tyr453-Tyr34	2.87	Hydrogen bond
	Asn487-Tyr83	2.92	Hydrogen bond
	Arg498-Glu38	2.79	Hydrogen bond
	Arg498-Glu38	2.77	Hydrogen bond
	Arg498-Glu38	3.05	Hydrogen bond
	Arg498-Glu38	2.97	Hydrogen bond
	Thr500-Asp355	2.75	Hydrogen bond
	Gly502-Lys353	2.86	Hydrogen bond
	Gly502-Lys353	2.86	Hydrogen bond
	Arg493-Glu35	3.36	Salt bridge
	Arg498-Glu38	2.77	Salt bridge

Comparatively important contacts have been lost during the simulation and thus binds the mAb weakly than the wild type. The interacting residues, bonding distance and type are given in Table 3.

Calculating the binding free energy (BFE) for biological molecules with the MM/GBSA and MM/PBSA methods are arguably the most frequently employed approach for accurately investigating the predicted docking conformation. These approaches demonstrate the binding stability of a interacting hotspots residues and the BFE and is less expensive than the wide-ranging alchemical free energy methods. Moreover, it is known to be more accurate than any rational scoring functions. Given this method's ability to shed light on the impact the structure, function,

Table 3
Post-simulation interactions analysis of the wild type-NTD and B.1.1.529-NTD in complex with mAb. The table shows the interacting residues, bonding distance and bond type.

Complex name	Interacting residues	Distance (Å)	Bond type
Wild Type-NTD	Glu31-Lys147	1.92	Hydrogen bond
	Asp55-Lys77	3.89	Hydrogen bond
	Lys77-Asp55	3.89	Hydrogen bond
	Tyr111-Leu249	2.66	Hydrogen bond
	Lys147-Glu31	1.92	Hydrogen bond
	GLU31-LYS147	1.91	Salt-bridge
	ASP55-LYS77	3.84	Salt-bridge
B.1.1.529-NTD	Arg153-Phe109	3.25	Hydrogen bond
	Asn143-Tyr111	3.20	Hydrogen bond
	Lys145-Pro53	2.55	Hydrogen bond
	Trp147-Gly56	2.88	Hydrogen bond

and interaction the mutations have on spike RBD binding to hACE2 and mAb binding to the NTD receptor, we used the MM/GBSA and MM/PBSA approaches. The estimated BFE and other measurements given by MM/GBSA for the wild type-RBD-hACE2, B.1.1.529-RBD-hACE2, wild-type-NTD-mAb, and B.1.1.529-NTD-mAb complexes are presented in Table 4. The wildtype-RBD-hACE2 complex has a vdW of −83.49 kcal/mol, an electrostatic energy of −585.73 kcal/mol, and a total binding free energy of −33.94 kcal/mol. These energy values for the B.1.1.529-RBD-hACE2 complex were −81.61 kcal/mol (vdW), −1458.24 kcal/mol (electrostatic), and −61.41 kcal/mol (total binding energy). The low TBE demonstrated by the B.1.1.529-RBD-hACE2 complex indicates that the B.1.1.529 variant interacts more effectively with hACE2 than the wild type, permitting the variant to spread more swiftly. Previous studies have demonstrated that a higher electrostatic energy is associated with different mutations, which increases the binding in different variants. Our docking and BFE energy results also strongly support previous findings [12,28,29]. The polar solvation and other values are given in Table 4 which demonstrate that the solvation energy is non-favorable in variants binding to ACE2, whereas gas-phase energy is key to the strong binding of the variants to ACE2. However, the BFE for the wild-type-NTD-mAb and B.1.1.529-NTD-mAb complexes revealed different results. The BFE for the wild-type-NTD-mAb complex was −33.66 kcal/mol and −26.80 kcal/mol for B.1.1.529-NTD-mAb complex, which consequently revealed that substitutions and deletions in the NTD reduce the binding of mAb, thus allowing the virus to evade the host's immune response. Our findings strongly corroborate with previous research demonstrating that the mutations and deletions in the NTD of B.1.618 variants resulted in immune evasion [29].

Moreover calculation of BFE using MM/PBSA further validated the MM/GBSA results. The vdW and electrostatic energies remained the same while the other features demonstrated differences. The wildtype-RBD-hACE2 complex had ΔG total = −18.72 kcal/mol, the B.1.1.529-RBD-hACE2 complex reported ΔG total = −27.27 kcal/mol. On the other hand, the wild-type-NTD-mAb and for the B.1.1.529-NTD-mAb complexes reported the ΔG total as −11.71 and −7.63 kcal/mol respectively. This demonstrates stronger agreement between the MM/GBSA and MM/PBSA approach which reflect the accuracy of the binding. Table 5 shows the MM/PBSA results.

4. Conclusions

A perpetual emergence of B.1.1.529 with 30 mutations in the spike protein is a somber gesture that the world is still under prolonged threat due to the ongoing pandemic. Thorough understanding of these variations and its implications in therapeutics development is needed. Our investigation to reveal the binding differences demonstrated that the key substitutions i.e., Asn417, Ser446, Arg493, Arg498 helps the new variants to bind more strongly than the wild type. The three CDR1–3 regions in the mAb are reported to abolish direct interactions with the NTD consequently produces escaping effect. Further investigation revealed that B.1.1.529 displayed a stable dynamic and reported a strong correlation with the previous reports where stability increasing mutations in the RBD were reported to enhance the binding. Moreover, the hydrogen bonding analysis and the total binding free energy further validated the results. While it must be proven conclusively, we believe that the immune responses elicited by presently available vaccines will be efficient in preventing against this variant due to certain commonalities in reported mutations in B.1.1.529 and other variants. This is the first study to provide basis for higher infectivity caused by B.1.1.529 and a strong impetus to develop novel drugs against the new SARS-CoV-2 variants.

Table 4
The BFE calculated by using MM/GBSA approach from the simulation trajectory of each complex. All the energies are represented in kcal/mol. The old represent the total binding free energy for each complex.

Parameters	Wild type-RBD	B.1.1.529-RBD	Wild type-NTD	B.1.1.529-NTD
vdW	−83.49	−81.61	−60.84	−65.39
Electrostatic	−585.73	−1458.24	−768.85	−186.16
EGB	647.04	1490.7	804.62	233.47
ESURF	−11.75	−12.24	−8.59	−8.72
ΔG solvated	635.29	1478.45	796.03	216.74
ΔG total	**−33.94**	**−61.41**	**−33.66**	**−26.80**

Table 5
The BFE calculated by using MM/PBSA approach from the simulation trajectory of each complex. All the energies are represented in kcal/mol. The old represent the total binding free energy for each complex.

Parameters	Wild type-RBD	B.1.1.529-RBD	Wild type-NTD	B.1.1.529-NTD
vdW	−83.49	−81.61	−60.84	−65.39
Electrostatic	−585.73	−1458.24	−768.85	−186.16
EPB	615.37	1451.8	785.58	202.58
ENPOLAR	−60.67	−62.16	−46.01	−48.77
ESPIDER	95.799	122.95	78.41	90.11
ΔG solvated	686.49	1512.59	840.05	258.93
ΔG total	**−18.72**	**−27.27**	**−11.71**	**−7.63**

Abbreviations

RBD receptor-binding domain
ACE2 Angiotensin-Converting Enzyme 2
vdW Van der Waal
GB generalized born
MMGBSA the molecular mechanics, the generalized Born model and solvent accessibility
MMPBSA the molecular mechanics Poisson-Boltzmann surface area
NTD N-terminal domain
mAb monoclonal antibodies
BFE binding free energy
ESURF surface area

Funding

Dong-Qing Wei is supported by grants from the Key Research Area Grant 2016YFA0501703 of the Ministry of Science and Technology of China, the National Science Foundation of China (Grant No. 32070662, 61832019, 32030063), the Science and Technology Commission of Shanghai Municipality (Grant No.: 19430750600), as well as SJTU JiRLMDS Joint Research Fund and Joint Research Funds for Medical and Engineering and Scientific Research at Shanghai Jiao Tong University (YG2021ZD02).

Availability of data and material

All the data is available on RCSB, UniProt and any simulation data would be provided on reasonable demand. The accession numbers to access this data are given in the manuscript.

Ethics approval and consent to participate

N/A.

Consent for publication

N/A.

Authors' contributions

Abbas Khan, Hira Waris, Memoona Rafique = Conceptualization, formal analysis, visualization, writing; Muhammad Suleman, Anwar Mohammad, Syed Shujait Ali, Taimoor Khan, Yasir Waheed =

validation, software, resources, initial drafting, Chenguang Liao and Dong-Qing Wei = visualization, validation, supervision, initial draft, final paper writing.

Declaration of competing interest

Authors declare there is no declaration of interest.

Data availability

Data will be made available on request.

Acknowledgements

The computations were partially performed at the PengCheng Lab. and the Center for High-Performance Computing, Shanghai Jiao Tong University.

References

[1] C. Wang, P.W. Horby, F.G. Hayden, G.F. Gao, A novel coronavirus outbreak of global health concern, Lancet 395 (10223) (2020) 470–473.
[2] K. Moelling, Within-host and between-host evolution in SARS-CoV-2-new variant's source, Viruses 13 (5) (2021).
[3] J.A. Plante, B.M. Mitchell, K.S. Plante, K. Debbink, S.C. Weaver, V.D. Menachery, The variant gambit: COVID-19's next move, Cell Host Microbe 29 (4) (2021) 508–515.
[4] J. Shang, Y. Wan, C. Luo, G. Ye, Q. Geng, A. Auerbach, F. Li, Cell entry mechanisms of SARS-CoV-2, Proc. Natl. Acad. Sci. U. S. A. 117 (21) (2020) 11727–11734.
[5] R. Wang, Y. Hozumi, C. Yin, G.W. Wei, Decoding SARS-CoV-2 transmission and evolution and ramifications for COVID-19 diagnosis, vaccine, and medicine, J. Chem. Inf. Model. 60 (2020) 5853–5865.
[6] S.R. Kannan, A.N. Spratt, A.R. Cohen, S.H. Naqvi, H.S. Chand, T.P. Quinn, C. L. Lorson, S.N. Byrareddy, K. Singh, Evolutionary analysis of the Delta and Delta plus variants of the SARS-CoV-2 viruses, J. Autoimmun. 124 (2021), 102715.
[7] S. Messali, A. Bertelli, G. Campisi, A. Zani, M. Ciccozzi, A. Caruso, F. Caccuri, A cluster of the new SARS-CoV-2 B. 1.621 lineage in Italy and sensitivity of the viral isolate to the BNT162b2 vaccine, J. Med. Virol. 93 (2021) 1–3.
[8] P.L. Wink, F.C.Z. Volpato, F.L. Monteiro, J.B. Willig, A.P. Zavascki, A.L. Barth, A. F. Martins, First identification of SARS-CoV-2 lambda (C. 37) variant in southern Brazil, Infect. Control Hosp. Epidemiol. (2021) 1–2.
[9] Z. Liu, L.A. VanBlargan, L.-M. Bloyet, P.W. Rothlauf, R.E. Chen, S. Stumpf, H. Zhao, J.M. Errico, E.S. Theel, M.J. Liebeskind, Identification of SARS-CoV-2 spike mutations that attenuate monoclonal and serum antibody neutralization, Cell Host Microbe 29 (3) (2021) 477–488, e4.
[10] T.-J. Yang, P.-Y. Yu, Y.-C. Chang, N.-E. Chang, Y.-X. Tsai, K.-H. Liang, P. Draczkowski, B. Lin, Y.-S. Wang, Y.-C. Chien, Structure-activity Relationships of B. 1.617 and Other SARS-CoV-2 Spike Variants, bioRxiv, 2021.
[11] M.K. Annavajhala, H. Mohri, P. Wang, M. Nair, J.E. Zucker, Z. Sheng, A. Gomez-Simmonds, A.L. Kelley, M. Tagliavia, Y. Huang, Emergence and expansion of SARS-CoV-2 B. 1.526 after identification in New York, Nature 597 (7878) (2021) 703–708.
[12] A. Khan, T. Zia, M. Suleman, T. Khan, S.S. Ali, A.A. Abbasi, A. Mohammad, D. Q. Wei, Higher infectivity of the SARS-CoV-2 new variants is associated with K417N/T, E484K, and N501Y mutants: an insight from structural data, J. Cell. Physiol. 236 (10) (2021) 7045–7057.
[13] C. Scheepers, J. Everatt, D.G. Amoako, H. Tegally, C.K. Wibmer, A. Mnguni, A. Ismail, B. Mahlangu, B.E. Lambson, S.I. Richardson, Emergence and Phenotypic Characterization of C. 1.2, A Globally Detected Lineage That Rapidly Accumulated Mutations of Concern, medRxiv, 2021, 2021.08. 20.21262342.
[14] S. Rao, M. Singh, The newly detected B. 1.1. 529 (Omicron) variant of SARS-CoV-2 with multiple mutations: implications for transmission, diagnostics, therapeutics, and immune evasion, DHR Proc. 1 (S5) (2021) 7–10.
[15] A. Li, A. Maier, M. Carter, T.Hugh Guan, Omicron and S-gene target failure cases in the highest COVID-19 case rate region in Canada, J. Med. Virol. 94 (December 2021) 1–3, n/a(n/a).
[16] A. Basu, A. Sarkar, U. Maulik, Molecular docking study of potential phytochemicals and their effects on the complex of SARS-CoV2 spike protein and human ACE2, Sci. Rep. 10 (1) (2020) 17699.
[17] N.A. Murugan, C.J. Pandian, J. Jeyakanthan, Computational investigation on Andrographis paniculata phytochemicals to evaluate their potency against SARS-CoV-2 in comparison to known antiviral compounds in drug trials, J. Biomol. Struct. Dyn. 39 (12) (2021) 4415–4426.
[18] A. Dwivedy, R. Mariadasse, M. Ahmad, S. Chakraborty, D. Kar, S. Tiwari, T. Majumdar, J. Jeyakanthan, B. Biswal, Characterization of the NiRAN Domain From RNA-dependent RNA Polymerase Provides Insights Into a Potential Therapeutic Target Against SARS-CoV-2, bioRxiv, 2021.
[19] C. Newsroom , CDC Statement on B. 1.1. 529 (Omicron Variant).
[20] M. Magrane, UniProt knowledgebase: a hub of integrated protein data, Database 2011 (2011).
[21] P.W. Rose, A. Prlić, A. Altunkaya, C. Bi, A.R. Bradley, C.H. Christie, L.D. Costanzo, J.M. Duarte, S. Dutta, Z. Feng, The RCSB protein data bank: integrative view of protein, gene and 3D structural information, Nucleic Acids Res. 45 (2016) D271–D281.
[22] R. Yan, Y. Zhang, Y. Li, L. Xia, Y. Guo, Q. Zhou, Structural basis for the recognition of SARS-CoV-2 by full-length human ACE2, Science 367 (6485) (2020) 1444–1448.
[23] X. Chi, R. Yan, J. Zhang, G. Zhang, Y. Zhang, M. Hao, Z. Zhang, P. Fan, Y. Dong, Y. Yang, Z. Chen, Y. Guo, J. Zhang, Y. Li, X. Song, Y. Chen, L. Xia, L. Fu, L. Hou, J. Xu, C. Yu, J. Li, Q. Zhou, W. Chen, A neutralizing human antibody binds to the N-terminal domain of the spike protein of SARS-CoV-2, Science 369 (6504) (2020) 650–655.
[24] T.D. Goddard, C.C. Huang, T.E. Ferrin, Software extensions to UCSF chimera for interactive visualization of large molecular assemblies, Structure 13 (3) (2005) 473–482.
[25] E.F. Pettersen, T.D. Goddard, C.C. Huang, G.S. Couch, D.M. Greenblatt, E.C. Meng, T.E. Ferrin, UCSF Chimera—a visualization system for exploratory research and analysis, J. Comput. Chem. 25 (13) (2004) 1605–1612.
[26] C. Dominguez, R. Boelens, A.M. Bonvin, HADDOCK: a protein− protein docking approach based on biochemical or biophysical information, J. Am. Chem. Soc. 125 (7) (2003) 1731–1737.
[27] P.I. Koukos, M.F. Reau, A.M. Bonvin, Shape-restrained Modelling of Protein-small Molecule Complexes With HADDOCK, bioRxiv, 2021.
[28] A. Khan D.-Q. Wei K. Kousar J. Abubaker S. Ahmad J. Ali F. Al-Mulla S.S. Ali N. Nizam-Uddin A.M. Sayaf , Preliminary structural data revealed that the SARS-CoV-2 B. 1.617 variant's RBD binds to ACE2 receptor stronger than the wild type to enhance the infectivity, ChemBioChem.
[29] A. Khan, J. Gui, W. Ahmad, I. Haq, M. Shahid, A.A. Khan, A. Shah, A. Khan, L. Ali, Z. Anwar, The SARS-CoV-2 B. 1.618 variant slightly alters the spike RBD–ACE2 binding affinity and is an antibody escaping variant: a computational structural perspective, RSC Adv. 11 (48) (2021) 30132–30147.
[30] R.A. Laskowski, PDBsum: summaries and analyses of PDB structures, Nucleic Acids Res. 29 (1) (2001) 221–222.
[31] D.A. Case, T.E. Cheatham III, T. Darden, H. Gohlke, R. Luo, K.M. Merz Jr., A. Onufriev, C. Simmerling, B. Wang, R.J. Woods, The Amber biomolecular simulation programs, J. Comput. Chem. 26 (16) (2005) 1668–1688.
[32] D.A. Pearlman, D.A. Case, J.W. Caldwell, W.S. Ross, T.E. Cheatham III, S. DeBolt, D. Ferguson, G. Seibel, P. Kollman, AMBER, a package of computer programs for applying molecular mechanics, normal mode analysis, molecular dynamics and free energy calculations to simulate the structural and energetic properties of molecules, Comput. Phys. Commun. 91 (1–3) (1995) 1–41.
[33] R. Salomon-Ferrer, D.A. Case, R.C. Walker, An overview of the Amber biomolecular simulation package, Wiley Interdiscip. Rev.: Comput. Mol. Sci. 3 (2) (2013) 198–210.
[34] J.C. Meza, Steepest descent, Wiley Interdiscip. Rev. Comput. Stat. 2 (6) (2010) 719–722.
[35] S.J. Watowich, E.S. Meyer, R. Hagstrom, R. Josephs, A stable, rapidly converging conjugate gradient method for energy minimization, J. Comput. Chem. 9 (6) (1988) 650–661.
[36] R. Salomon-Ferrer, A.W. Götz, D. Poole, S. Le Grand, R.C. Walker, Routine microsecond molecular dynamics simulations with AMBER on GPUs. 2. Explicit solvent particle mesh ewald, J. Chem. Theory Comput. 9 (9) (2013) 3878–3888.
[37] D.R. Roe, T.E. Cheatham III, PTRAJ and CPPTRAJ: software for processing and analysis of molecular dynamics trajectory data, J. Chem. Theory Comput. 9 (7) (2013) 3084–3095.
[38] A. Khan, A.C. Kaushik, S.S. Ali, N. Ahmad, D.-Q. Wei, Deep-learning-based target screening and similarity search for the predicted inhibitors of the pathways in Parkinson's disease, RSC Adv. 9 (18) (2019) 10326–10339.
[39] A. Ali, M.T. Khan, A. Khan, S. Ali, S. Chinnasamy, K. Akhtar, A. Shafiq, D.-Q. Wei, Pyrazinamide resistance of novel mutations in pncA and their dynamic behavior, RSC Adv. 10 (58) (2020) 35565–35573.
[40] A. Khan, M.T. Khan, S. Saleem, M. Junaid, A. Ali, S.S. Ali, M. Khan, D.-Q. Wei, Structural insights into the mechanism of RNA recognition by the N-terminal RNA-binding domain of the SARS-CoV-2 nucleocapsid phosphoprotein, computational and structural, Biotechnol. J. 18 (2020) 2174–2184.
[41] M. Tahir ul Qamar, S. Ahmad, A. Khan, M.U. Mirza, S. Ahmad, A. Abro, L.-L. Chen, A. Almatroudi, D.-Q. Wei, Structural probing of HapR to identify potent phytochemicals to control Vibrio cholera through integrated computational approaches, Comput. Biol. Med. 138 (2021) 1–10.
[42] Y. Wang, A. Khan, A. Chandra Kaushik, M. Junaid, X. Zhang, D.-Q. Wei, The systematic modeling studies and free energy calculations of the phenazine compounds as anti-tuberculosis agents, J. Biomol. Struct. Dyn. 37 (15) (2019) 4051–4069.
[43] H. Sun, Y. Li, S. Tian, L. Xu, T. Hou, Assessing the performance of MM/PBSA and MM/GBSA methods. 4. Accuracies of MM/PBSA and MM/GBSA methodologies evaluated by various simulation protocols using PDBbind data set, Phys. Chem. Chem. Phys. 16 (31) (2014) 16719–16729.
[44] S. Gautam, L. Hens, in: COVID-19: Impact by and on the Environment, Health and Economy, Springer, 2020, pp. 1–2.
[45] A. Khan, J. Gui, W. Ahmad, I. Haq, M. Shahid, A.A. Khan, A. Shah, A. Khan, L. Ali, Z. Anwar, M. Safdar, J. Abubaker, N.N. Uddin, L. Cao, D.-Q. Wei, A. Mohammad, The SARS-CoV-2 B.1.618 variant slightly alters the spike RBD–ACE2 binding affinity and is an antibody escaping variant: a computational structural perspective, RSC Adv. 11 (48) (2021) 30132–30147.
[46] A. Khan, T. Khan, S. Ali, S. Aftab, Y. Wang, W. Qiankun, M. Khan, M. Suleman, S. Ali, W. Heng, SARS-CoV-2 new variants: characteristic features and impact on the efficacy of different vaccines, Biomed. Pharmacother. 112176 (2021).

[47] M. Suleman, Q. Yousafi, J. Ali, S.S. Ali, Z. Hussain, S. Ali, M. Waseem, A. Iqbal, S. Ahmad, A. Khan, Bioinformatics analysis of the differences in the binding profile of the wild-type and mutants of the SARS-CoV-2 spike protein variants with the ACE2 receptor, Comput. Biol. Med. 138 (2021), 104936.
[48] I. Celik, R. Yadav, Z. Duzgun, S. Albogami, A.M. El-Shehawi, R. Fatimawali, T. E. Idroes, T.B.Emran Tallei, Interactions of the receptor binding domain of SARS-CoV-2 variants with hACE2: insights from molecular docking analysis and molecular dynamic simulation, Biology 10 (9) (2021) 880.
[49] J. de Andrade, P.F.B. Gonçalves, P.A. Netz, Why does the novel coronavirus spike protein interact so strongly with the human ACE2? A thermodynamic answer, ChemBioChem 22 (5) (2021) 865–875.
[50] T.N. Starr, A.J. Greaney, S.K. Hilton, D. Ellis, K.H. Crawford, A.S. Dingens, M. J. Navarro, J.E. Bowen, M.A. Tortorici, A.C. Walls, Deep mutational scanning of SARS-CoV-2 receptor binding domain reveals constraints on folding and ACE2 binding, Cell 182 (5) (2020) 1295–1310, e20.
[51] Thaddeus M. Davenport, J. Gorman, M.G. Joyce, T. Zhou, C. Soto, M. Guttman, S. Moquin, Y. Yang, B. Zhang, Nicole A. Doria-Rose, S.-L. Hu, John R. Mascola, Peter D. Kwong, Kelly K. Lee, Somatic hypermutation-induced changes in the structure and dynamics of HIV-1 broadly neutralizing antibodies, Structure 24 (8) (2016) 1346–1357.
[52] V. Ovchinnikov, J.E. Louveau, J.P. Barton, M. Karplus, A.K. Chakraborty, Role of framework mutations and antibody flexibility in the evolution of broadly neutralizing antibodies, elife 7 (2018), e33038.
[53] D. Chen, N. Oezguen, P. Urvil, C. Ferguson, S. Dann, T. Savidge, Regulation of protein-ligand binding affinity by hydrogen bond pairing, Sci. Adv. 2 (3) (2016), e1501240.
[54] J.D. Chodera, D.L. Mobley, Entropy-enthalpy compensation: role and ramifications in biomolecular ligand recognition and design, Annu. Rev. Biophys. 42 (2013) 121–142.
[55] R. Patil, S. Das, A. Stanley, L. Yadav, A. Sudhakar, A.K. Varma, Optimized hydrophobic interactions and hydrogen bonding at the target-ligand interface leads the pathways of drug-designing, PloS one 5 (8) (2010), e12029.
[56] T.S. Olsson, J.E. Ladbury, W.R. Pitt, M.A. Williams, Extent of enthalpy–entropy compensation in protein–ligand interactions, Protein Sci. 20 (9) (2011) 1607–1618.